ACS APPLIED MATERIALS & INTERFACES

Research Article

www.acsami.org

A Facile in Situ Self-Assembly Strategy for Large-Scale Fabrication of CHS@MOF Yolk/Shell Structure and Its Catalytic Application in a Flow System

Hongyi Gao, Yi Luan, Kullapat Chaikittikul, Wenjun Dong,* Jie Li, Xiaowei Zhang, Dandan Jia, Mu Yang, and Ge Wang*

Beijing Key Laboratory of Function Materials for Molecule & Structure Construction, School of Materials Science and Engineering, University of Science and Technology Beijing, 30 Xueyuan Road, Beijing 100083, P. R. China

Supporting Information

ABSTRACT: A hierarchical yolk/shell copper hydroxysulfates@MOF (CHS@MOF, where MOF = metal−organic frameworks) structure was fabricated from a homogeneous yolk/shell CHS template composed of an active shell and a stabilized core via a facile self-template strategy at room temperature. The active shell of the template served as the source of metal ion and was in situ transformed into a well-defined MOF crystal shell, and the relatively stabilized core retained its own nature during the formation of the MOF shell. The strategy of in situ transformation of CHS shell to MOF shell avoided the self-nucleation of MOF in the solution and complex multistep procedures. Furthermore, a flow reaction system using CHS@MOF as self-supported stationary-phase catalyst was developed, which demonstrated excellent catalytic performance for aldehyde acetalization with ethanol, and high yields and selectivities were achieved under mild conditions.

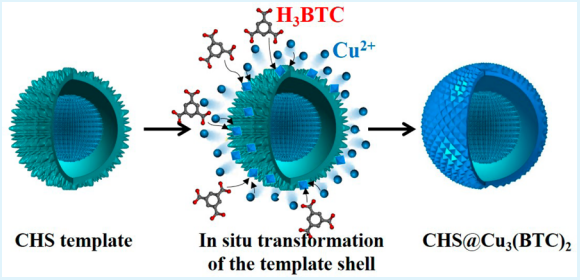

KEYWORDS: *yolk/shell, CHS@MOF, self-template, in situ transformation*

1. INTRODUCTION

Controllable fabrication of hierarchical structure is one effective way to realize the distinctively collective property and extensive potential of two or more functional components.[1−4] In particular, functional core/shell or yolk/shell structures not only avoid the aggregation of the cores with high surface energy and preserve their chemical activity but also greatly improve the multifunctionality of the nanostructures.[5,6] Recently, functional microparticles/nanoparticles@metal−organic framework (MP/NP@MOF) core/shell or yolk/shell structures have attracted considerable research interest due to their synergies obtained by integrating functions of the MOF shell and MP/NP cores.[7,8] The high surface area, diverse structural topologies, adjustable pore size, and tunable chemical properties of MOF shell, together with the functionality of MP/NP cores such as magnetic, optical, and catalytic properties, can be effectively integrated. Until now, MP/NP@MOF such as metal@MOF,[9,10] metal oxide@MOF,[11] polymer@MOF,[12,13] inorganic material@MOF,[14,15] and MOF@MOF[16] have been successfully achieved and show potential applications in catalysis, drug and gene delivery, sensing, gas storage, and gas separation.[17] For example, Zhang et al. prepared core/shell silica@$Cu_3(BTC)_2$ (BTC = 1,3,5-benzenetricarboxylate) composite microspheres via a step-by-step approach and demonstrated that silica@$Cu_3(BTC)_2$ as packing materials can realize fast and efficient separation for liquid chromatography.[14] Qiu et al. synthesized core/shell Au@MIL-100(Fe) with enhanced catalytic performance and core/shell Fe_3O_4@$Cu_3(BTC)_2$ with magnetic recovery capability.[10,11] Recently, Kuo et al. fabricated an interesting yolk/shell nanocrystal@ZIF-8,[17] which integrates the functions of the microporous shell, the catalytic core, and the cavity between and offers greater prospects of optimizing the performance of the composite materials.[18]

Until now, significant progress has been achieved in the preparation of hierarchical MP/NP@MOF structures, and the synthetic methods are mainly classified into two categories. The first is the incorporation of MP/NP into MOF.[19−27] The incorporation of MP/NP into MOF often damages the porous structure of the MOF, and the morphology and size of the MP/NP is uncontrollable. The second is the coating of MOF shell on modified MP/NP core.[28−33] The coating strategy usually requires additional surface modifications on the MP/NP to confine the nucleation and growth of MOF, so the self-nucleation of MOF in solution is difficult to avoid. Usually, a yolk/shell MP/NP@MOF structure is fabricated via a step-by-step coating strategy with an additional selective etching procedure,[17] which makes the synthesis process complicated and inefficient. In addition, traditional multistep procedures hinder the large-scale synthesis of yolk−shell-type structures. So it is highly desirable to develop a facile and rapid method for

Received: November 18, 2014
Accepted: February 13, 2015
Published: February 13, 2015

DOI: 10.1021/am508079j
ACS Appl. Mater. Interfaces 2015, 7, 4667−4674

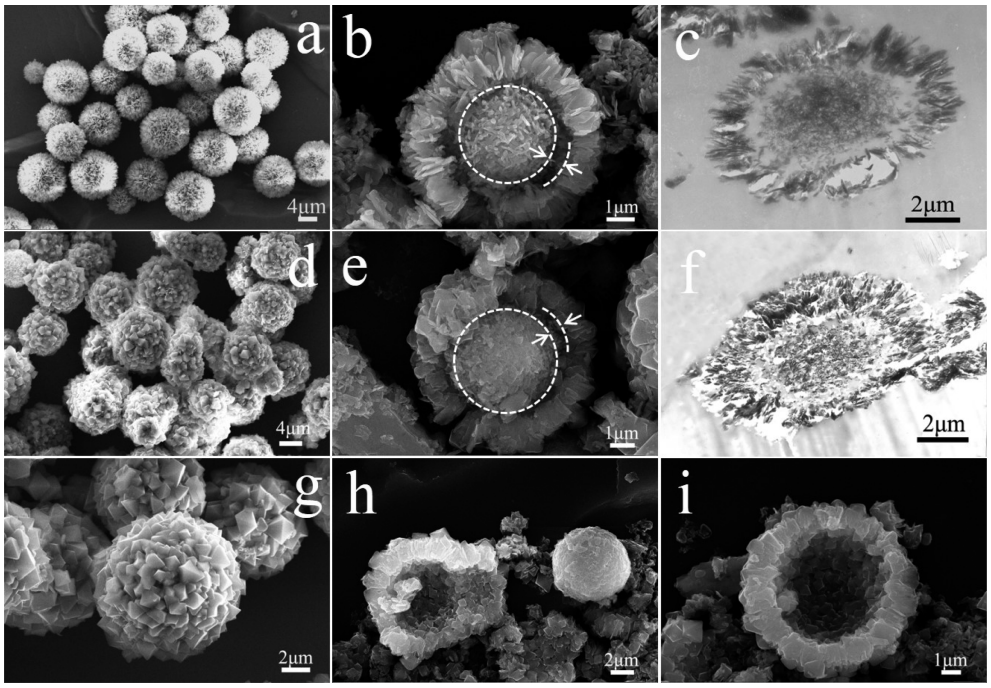

Figure 1. (a, b) SEM images and (c) cross-section TEM image of the as-prepared yolk/shell CHS template. (d, e, g) SEM images and (f) cross-section TEM images of the yolk/shell CHS@$Cu_3(BTC)_2$ microspheres. The circle marked gives the outline of the core, and the arrow shows the interstitial gap between the core and shell in (b, e). (h, i) SEM images of $Cu_3(BTC)_2$ shell separated from the core.

scalable fabrication of yolk/shell MP/NP@MOF structures under mild conditions.

In this paper, a novel self-template method was developed for large-scale synthesis of the MP@MOF yolk/shell structure.[34,35] First, the homogeneous yolk/shell template with active shell and relatively stable core was designed and synthesized. The active shell served as the source of metal ion and was in situ converted to MOF shell, while the relatively stabilized core retained its own nature during the formation of the MOF shell. The MOF shell of the yolk/shell MP@MOF products was assembled from well-defined crystal subunits. Importantly, the size of the subunit of the MOF shell could be controlled by varying the solvent composition. CHS has been proven to be an excellent catalyst for a variety of catalytic reactions, such as olefin oxidation and phenol oxidation, with advantages of low cost, environmental friendly, and high activity. But the reusability of CHS still needs to be improved, which limits its potential application.[36,37] The yolk/shell CHS@MOF structure achieves cooperative catalytic activity and good reusability by integrating not only the CHS core with high catalytic activity but also the MOF shell with large surface area and high porosity. Furthermore, the solid-core-porous-shell structure of the CHS@MOF make it ideal for self-supported catalyst in a flow catalysis system due to the advantage of being easily packed and immobilized. A flow reaction system using CHS@$Cu_3(BTC)_2$ as self-supported stationary-phase was developed and evaluated for aldehydes acetalization reaction, which demonstrated the enhanced catalytic properties of the CHS@$Cu_3(BTC)_2$ and the economical and environmentally processes of the as-prepared flow catalytic reactor.

2. EXPERIMENTAL SECTION

Materials. Copper sulfate pentahydrate, absolute ethanol, and *N*,*N*-dimethylformamide (DMF) were purchased from the Beijing Chemical Reagent Company. 1,3-Propanediamine and trimesic acid were supplied by Alfa Aesar. All reagents were of analytical grade and used without further purification.

Preparation of Yolk/Shell CHS Template. The synthesis of the yolk/shell CHS template was carried out by an amplified complexed-precipitation method according to our previous work.[36] In a typical procedure, 0.30 L of 1,3-propanediamine (0.24 mol/L) was added into 0.40 L of $CuSO_4$ solution (0.75 mol/L). The mixed solution was kept still for 10 min at room temperature. Then the green precipitate was obtained by centrifugation, washed with deionized water twice and ethanol once, and dried at 40 °C for 12 h. Then the yolk/shell CHS templates were obtained.

Preparation of Yolk/Shell CHS@MOF. Yolk/shell CHS templates (10.00 g) were added into 0.34 L of mixed ethanol and water solution (ethanol: 0.16 L, water: 0.18 L) under stirring. Then another 0.30 L of ethanol solution of trimesic acid (0.05 mol/L) was added into the above solution. The mixtures were stirred for 30 min at room temperature. Afterward, the products were recovered by centrifugation, washed with ethanol three times, and dried at 40 °C for 12 h. Then the yolk/shell CHS@$Cu_3(BTC)_2$ was obtained. To investigate the effect of the reaction temperature on the formation of CHS@$Cu_3(BTC)_2$, the products were prepared at 50 and 80 °C, respectively. To investigate the effect of solvent composition on the formation of CHS@$Cu_3(BTC)_2$, the mixed ethanol and water solution was replaced by water, DMF, and ethanol.

Characterization. The morphology, structure, and element mapping of the as-prepared products were investigated by scanning electron microscopy (SEM, ZEISS SUPRA55) and transmission electron microscopy (TEM, JEOL JEM-100CX II). The phase composition of the products was characterized by X-ray powder diffraction (XRD, M21X, Cu Kα radiation, λ = 0.1542 nm). Fourier transform infrared spectroscopy (FTIR) was collected on a Nicolet 6700 Fourier spectrometer using KBr pellets technique. The thermal decomposition behavior of the products was investigated with thermogravimetric experiments (TG, Netzsch STA449F3) from room temperature to 900 °C at a rate of 10 °C/min in N_2 atmosphere. The Brunauer–Emmett–Teller (BET) surface area and porosity of the as-synthesized products were characterized by nitrogen sorption–desorption isotherms at 77 K using a Micromeritics ASAP

DOI: 10.1021/am508079j
ACS Appl. Mater. Interfaces 2015, 7, 4667–4674

2420 adsorption analyzer. The pore size distribution was calculated using the Horvath–Kawazoe (HK) method.

Catalytic Tests and Flow Reaction System. In a typical procedure, 50 mg of catalysts, 1.0 mmol of substrate, and 5.0 mL of ethanol were added into a 25 mL round-bottomed flask. Then the mixture was stirred at room temperature for 1 h. At the end of the reaction, the products were isolated by centrifugation and analyzed by gas chromatography–mass spectrometry (GC-MS, Agilent7890/5975C-GC/MSD) to determine the catalytic efficiency. The flow reactor was equipped with CHS@$Cu_3(BTC)_2$ as self-supported catalyst and conducted the catalytic reaction at room temperature. A filtration was first packed on the bottom of the tubular reactor. To pack the cartridges (~400 mm) of the flow reactor, CHS@$Cu_3(BTC)_2$ (4 g) were first suspended in 100 mL of ethanol, then the slurry was injected into the column of the reactor using a syringe. The mixture of the aldehydes and ethanol with a molar ratio of 1:80 was directly injected into the inlet port of the flow reactor at a flow rate of 0.05 mL/min. All the tests were performed under room temperature (25 °C). Then the product was collected at the discharge port in a single pass and analyzed by gas chromatography–mass spectrometry (GC-MS, Agilent7890/5975C-GC/MSD) to determine the catalytic efficiency.

3. RESULTS AND DISCUSSION

3.1. In Situ Transformation of Yolk/Shell CHS Template to Yolk/Shell CHS@$Cu_3(BTC)_2$. The CHS yolk/shell template was prepared with an amplified complexed-precipitation method according to our previous work.[36] 1,3-Propanediamine was first added into the copper sulfate solution at room temperature. Then the hierarchical yolk/shell CHS microspheres were obtained after a 10 min reaction. As shown in Figure 1a,b, the CHS template is yolk/shell microsphere structures with a size of 7–9 μm, and the inner core (~5 μm) is encapsulated in a nanosheet-assembled shell with a thickness of 1 μm. The core is assembled from closely aggregated tiny nanoplatelets, each with a thickness of ~10 nm, and the outer shell is composed of closely packed nanosheets, each with a thickness of ~100 nm. The interstitial gap between the core and shell is about several hundred nanometers. The circle in Figure 1b implies the outline of the CHS core, while the arrow shows the interstitial gap between. TEM characterization further confirms the yolk/shell structure with the closely aggregated inner core and relatively loosely assembled outer shell (Figure 1c). The yolk/shell CHS template was formed from a metastable core/shell microsphere, and the gap between was caused by mass transfer from the core to shell, which was similar to the Ostwald ripening process.[36]

The yolk/shell CHS@$Cu_3(BTC)_2$ was fabricated by in situ conversion of the template shell to well-defined MOF crystal shell. When trimesic acid was added into the mixed water and ethanol dispersion of yolk/shell CHS template, the solution color changed from light green to light blue within 10 s, indicating the formation of the $Cu_3(BTC)_2$.[38] Nearly 20 g of products were obtained (Supporting Information, Figure S1). The nanosheets in the shell of the template are transformed into uniform and well-defined octahedral crystals with sizes of ~1 μm, and the octahedral crystals are assembled into the closely arranged MOF shell (Figure 1d–i). As can be seen from Figure 1e, the circle and arrow show that the CHS@$Cu_3(BTC)_2$ retains the yolk/shell structure. After a vigorous ultrasonication treatment, some microspheres are broken, and the MOF shells are separated from the inner core (Figure 1h,i), demonstrating the yolk/shell feature of the products. The elemental mapping images of a broken microsphere (Supporting Information, Figure S2) illustrate that C element distributed in the edge (the area out of the oval) is attributed to the formation of the $Cu_3(BTC)_2$ shell. The Cu, O, and S densely distributed in the center of the yolk/shell structure (the area in the circle) indicate the preservation of the CHS core. The size of the hierarchical CHS@$Cu_3(BTC)_2$ can be easily adjusted from 4 to 10 μm by applying this synthesis method with different sized yolk/shell CHS template (Supporting Information, Figure S3). Notably, the synthesis process can be conducted by simply mixing the dispersion of the template and organic ligands using water and alcohol as a solvent, and the reaction was completed within 30 min at room temperature producing gram-scale quantities in a 1 L beaker. This self-template method shows the advantages of being fast, mild, scalable, inexpensive, and environmentally friendly, and has great potential for the practical synthesis of yolk/shell CHS@$Cu_3(BTC)_2$.

The transformation from CHS template to CHS@$Cu_3(BTC)_2$ was investigated by XRD and nitrogen adsorption/desorption measurements (Figure 2). The diffraction

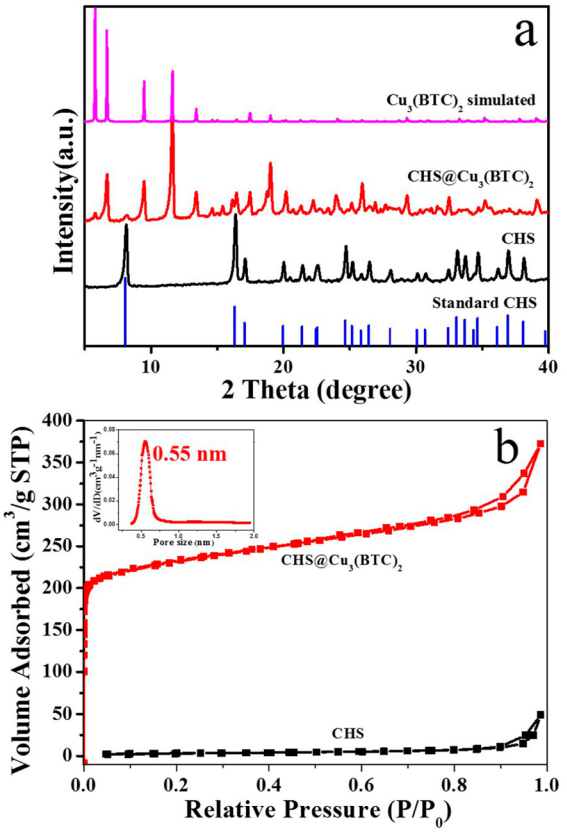

Figure 2. (a) XRD patterns and (b) N_2 sorption–desorption isotherms of the as-prepared CHS template and CHS@$Cu_3(BTC)_2$ microspheres.

peaks of the template are attributable to CHS ($Cu_{2.5}SO_4(OH)_3 \cdot 2H_2O$, JCPDS: No. 51–0321, CHS refers to $Cu_{2.5}SO_4(OH)_3 \cdot 2H_2O$ in this paper).[36] When the shell of the CHS template is converted to octahedral crystal shell, new diffraction peaks at 5.7°, 6.7°, 9.5°, 11.6°, 13.4°, 17.4°, and 19.0° appear, which are identical to the peaks of the calculated $Cu_3(BTC)_2$.[38,39] The diffraction peaks of the CHS can still be observed due to the existence of the stabilized CHS core. The specific surface area of the yolk/shell CHS template is ~9.4 m^2/g. The isotherms appear between type III plots, characteristic of the macropores,

DOI: 10.1021/am508079j
ACS Appl. Mater. Interfaces 2015, 7, 4667–4674

and type IV plots, characteristic of mesopores. The macropores and mesopores mainly originate from the loosely assembled nanosheets of the shell and the closely aggregated tiny nanoplatelets of the core.[35] The BET surface area of the CHS@$Cu_3(BTC)_2$ composite reached a high value of ~572.0 m^2/g when the CHS shell is converted to MOF shell. The isotherm curves appear between type I plots, characteristic of the micropores, and type IV plots, characteristic of mesopores. The pore size of the final product distributes narrowly around 0.55 nm. The high surface area and the micropore structure of the CHS@$Cu_3(BTC)_2$ are mainly due to the formation of the MOF shell. The chemical composition of the CHS@$Cu_3(BTC)_2$ product is further characterized by FTIR spectroscopy and thermogravimetric analysis (TGA) (Supporting Information, Figures S4 and S5). Sharp peaks of the FTIR spectra at 1450 and 1373 cm^{-1} are attributable to structural vibrations of the aromatic C═C bond and C−O bond of the $Cu_3(BTC)_2$ shell. The thermal decomposition behavior of the CHS@$Cu_3(BTC)_2$ product, with a weight loss within a range of 300−450 °C, also confirms the formation of the $Cu_3(BTC)_2$.[40]

3.2. Formation Pathway of the Yolk/Shell CHS@$Cu_3(BTC)_2$. The transformation from CHS shell to $Cu_3(BTC)_2$ crystal shell is a crucial issue in the elaboration of hierarchical CHS@$Cu_3(BTC)_2$ composite. To better understand this in situ conversion process, the microstructure and phase constitution of samples formed at different reaction times were investigated in detail. As shown in Figure 3a−d, after

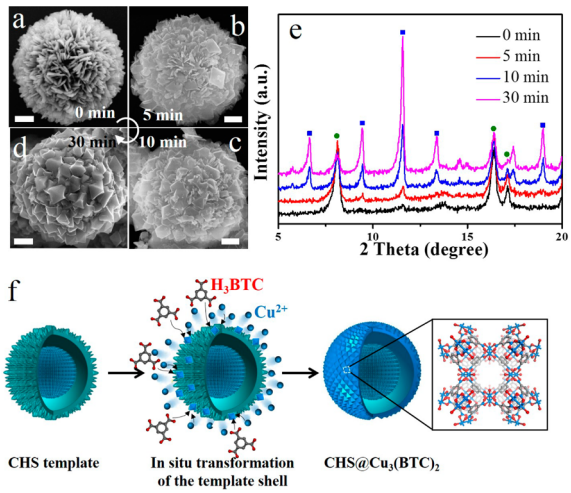

Figure 3. SEM images of CHS@$Cu_3(BTC)_2$ composites obtained with different reaction times: (a) 0 min, (b) 5 min, (c) 10 min, (d) 30 min. All the scale bars are 1 μm. (e) XRD patterns corresponding to samples obtained after different reaction times. (f) The corresponding schematic illustration of the formation of yolk/shell CHS@$Cu_3(BTC)_2$ microspheres.

trimesic acid is added into the dispersed solution of the yolk/shell CHS template for 5 min, sporadic octahedral crystals start to appear on the nanoplate shell of the CHS template. The template acts as the source of metal ions to provide Cu^{2+} for the MOF formation, which can be evidenced by the disappearance of the nanosheet shell of the template.[38] After 10 min of reaction, most of the assembled nanosheets of the template shell are converted to truncated octahedral crystals. When the reaction time reaches 30 min, all the nanosheet shell of the template are completely transformed to well-structured octahedron shell.

The transformation of the phase constitution of the samples is also characterized by XRD. For the pure CHS template, only the characteristic peaks (circle icon) of CHS at 8.1°, 16.4°, and 17.2° are shown (Figure 3e). With the increase of the reaction time after the trimesic acid was added into the solution, the diffraction peaks (square icons) of the $Cu_3(BTC)_2$ at 6.7°, 9.5°, 11.6°, 13.4°, and 19.0° appear, and the intensity gradually increases. The XRD characterization clearly shows the evolution from the CHS template to CHS@$Cu_3(BTC)_2$.

Pérez-Ramírez and co-workers successfully fabricated $Cu_3(BTC)_2$ using insoluble copper hydroxide as copper precursor for the first time. The copper hydroxide provided active sites to induce the MOF nucleation on its surface and was completely converted into $Cu_3(BTC)_2$. The conversion process was promoted by the acid−base interaction of the trimesic acid and copper hydroxide.[38] As for the yolk/shell CHS template composed of an active shell and a stabilized core, the shell serves as the source of copper and provide active sites for the MOF nucleation,[41,42] the core maintains its own nature very well attributed to its higher stability than the shell. The in situ conversion process of the CHS@$Cu_3(BTC)_2$ can be described in Figure 3f. When trimesic acid is added into the dispersed solution of the template, the nanosheets in the CHS shell produce active sites to induce the MOF nucleation on its surface, then the CHS structure is rearranged and converted to $Cu_3(BTC)_2$ crystal. With the consumption of the Cu^{2+} and the crystallization of $Cu_3(BTC)_2$, the CHS shell is gradually converted to $Cu_3(BTC)_2$ octahedral crystal shell. Further, the acid−base interaction between the trimesic acid and CHS also promoted the conversion process. Then the CHS@$Cu_3(BTC)_2$ yolk/shell structure is constructed.[38] Interestingly, no single $Cu_3(BTC)_2$ crystals are observed in the solution, which confirms that the nucleation and growth of the MOF crystals are strictly confined on the template shell. Three different synthetic reactions are involved in this facile self-template method, namely, (I) the fabrication of a yolk/shell CHS template, (II) the in situ conversion of CHS shell built from assembled nanosheets, and (III) the formation of MOF shell assembled from well-defined crystals. During the formation process of the CHS@$Cu_3(BTC)_2$, the active shell of the template serves as a source of metal ion and in situ converts to MOF shell, while the relatively stable core retains its own nature.

3.3. Key Factors in Formation of the Yolk/Shell CHS@MOF. Usually, the step-by-step coating strategy requires the introduction of additional metal ions. However, in the present work the Cu^{2+} for the formation of $Cu_3(BTC)_2$ were originated from the sacrificial CHS template in our self-template method. So the formation pathway of $Cu_3(BTC)_2$ mainly depended on the chemical reaction equilibrium between the release rate of Cu^{2+} and its coordination rate with the BTC ligands, which were controlled by kinetics and were closely related to the reaction environment. Systematic experiments were designed to investigate the effects of reactive conditions, such as the temperature and solvent composition, on the evolution of CHS@$Cu_3(BTC)_2$. When CHS@$Cu_3(BTC)_2$ was prepared at 50 °C, only a few large $Cu_3(BTC)_2$ crystals attached to the surface of the CHS core (Figure 4a). High temperature (80 °C) significantly accelerated the release rate of Cu^{2+} originating from the CHS shell, and the size of the $Cu_3(BTC)_2$ crystals grew larger (Figure 4b). The abundant Cu^{2+} in the solution promoted the growth of the $Cu_3(BTC)_2$ crystals and gave rise to the large size of the $Cu_3(BTC)_2$ crystals near the CHS core.

DOI: 10.1021/am508079j
ACS Appl. Mater. Interfaces 2015, 7, 4667−4674

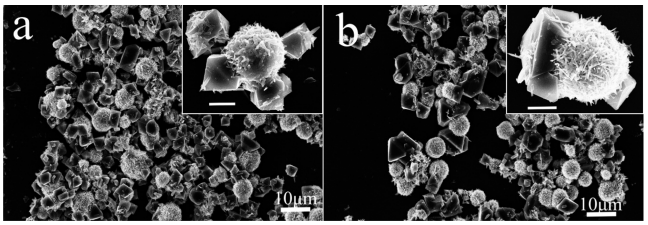

Figure 4. SEM images of products prepared at (a) 50 °C and (b) 80 °C. Both the scale bars in the inset are 2 μm.

Note that the retained CHS core confirmed that the core of the template was more stable than the shell.

The effects of different solvents, such as water, DMF, and ethanol, on the formation of the MOF shell were also investigated. When water was used as the solvent, the octahedron subunit size of the $Cu_3(BTC)_2$ shell increased to ~1.8 μm, nearly twice the size (~1 μm) of the products synthesized using a mixed water and ethanol solution (Figure 5a,b). When DMF was used as the solvent, the size of the

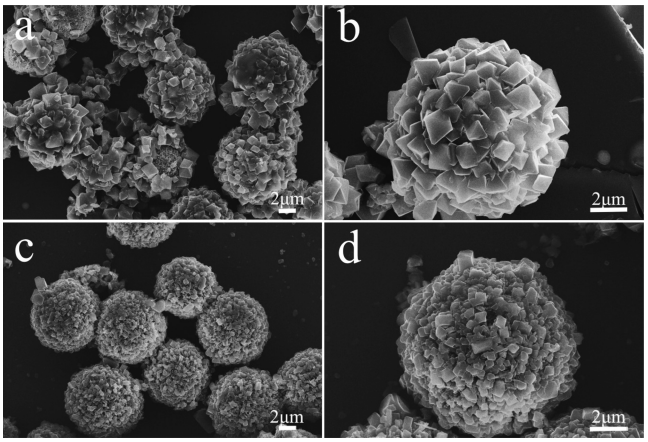

Figure 5. SEM images of the products prepared using (a, b) water and (c, d) DMF as solvent.

$Cu_3(BTC)_2$ crystal subunit decreased to ~700 nm (Figure 5c,d). Ethanol solvent only resulted in a few octahedron crystals on the template surface, and most of the nanosheet shell of the template was still retained (Supporting Information, Figure S6). As the polarity (dielectric constant) of water (80.1), mixed water and ethanol, DMF (36.7), and ethanol (24.5) gradually decreased, it can be concluded that the size of the $Cu_3(BTC)_2$ crystal subunit decreased with the polarity of the solvent. Previous research shows that high-polarity solvent can promote the dissociation of the organic ligands and increase the acidity of the reaction mixture.[35] So, in the present work, when water was used as solvent, the relatively highly acidic environment promoted the release of Cu^{2+} from the template. Then high concentration of Cu^{2+} and abundant BTC ligands gave rise to the quicker growth rate of MOF crystal and the larger size of the final $Cu_3(BTC)_2$ crystal subunit.

3.4. Catalytic Properties and Flow Reaction System Using CHS@MOF as Self-Supported Catalyst. Acetalization is one of the essential reactions for protecting carbonyl groups in a various organic syntheses.[43] Initially, acetalization reaction of benzaldehyde with ethanol was chosen as a model reaction to probe the activity of the CHS@$Cu_3(BTC)_2$ catalyst. The catalytic reactions were conducted at room temperature (25 °C) for 1 h. The benzaldehyde was converted to benzaldehyde diethyl acetal with a good yield (up to 88%) and high selectivity (up to 99%) (Table 1, entry 1). Compared

Table 1. Acetalization of Benzaldehyde Using Different Catalysts[a]

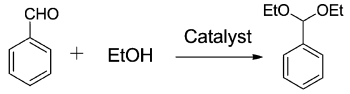

entry	sample	conversion (%)	selectivity (%)
1	CHS@$Cu_3(BTC)_2$	88	100
2		0	0
3	CHS	80	100
4	$Cu_3(BTC)_2$	17	100

[a]Reaction conditions: 1.0 mmol of benzaldehyde, 5.0 mL of ethanol, 50 mg of CHS@$Cu_3(BTC)_2$ (other catalysts with the same Cu content as the CHS@$Cu_3(BTC)_2$), room temperature (25 °C), 1 h.

with other catalysts reported for the acetalization reaction of aldehydes with ethanol, such as $RuCl_3$ and $CoCl_2$,[44,45] the CHS@$Cu_3(BTC)_2$ catalyst shows better catalytic activity. To investigate the catalytic effects of the CHS@$Cu_3(BTC)_2$, several control experiments were also conducted. A blank experiment shows that there was no reaction between benzaldehyde and ethanol after 1 h at room temperature (Table 1, entry 2). When CHS template and pure $Cu_3(BTC)_2$ were used as the catalysts, the conversion of benzaldehyde was 80% and 17%, respectively (Table 1, entries 3 and 4). For the yolk/shell copper CHS@$Cu_3(BTC)_2$, it is the CHS core that promotes the acetalization of benzaldehyde. The $Cu_3(BTC)_2$ shell with large surface area functions as the reactor, which provides multiple transportation channels for the reactants to access the catalytically active CHS surface. The reactants are restricted in a limited space between the core and shell of CHS@$Cu_3(BTC)_2$, which accelerated the catalytic reaction rate.

Furthermore, the recyclability of the CHS@$Cu_3(BTC)_2$ and CHS was also investigated. After being recycled more than five times, the efficiency of CHS@$Cu_3(BTC)_2$ catalyst maintains well (the conversion of benzaldehyde (80%) and the selectivity of benzaldehyde diethyl acetal (>99%)). On the other hand, for the CHS catalyst the conversion of benzaldehyde decreased significantly to 28% (Supporting Information, Figure S7). The morphologies and crystal structures of the used CHS and CHS@$Cu_3(BTC)_2$ were not changed (Supporting Information, Figures S8 and S9). After the CHS and CHS@$Cu_3(BTC)_2$ were filtered from the reaction mixture, the solution was stirred, and after a certain time it was analyzed by GC-MS analysis to verify the stability of catalysts. Results showed that the conversion of benzaldehyde increased from 46% to 69% after the CHS was removed, while the conversion of benzaldehyde only increased from 54% to 62%, indicating the higher stability of CHS@$Cu_3(BTC)_2$ than pure CHS (Supporting Information, Figure S10). The catalytic performance of CHS and CHS@$Cu_3(BTC)_2$ products after three months of storage in air was also studied; the conversion of benzaldehyde decreases to 18% for CHS, while the conversion of benzaldehyde still retains 83% for CHS@$Cu_3(BTC)_2$. The XRD result shows that the phase of the CHS is transformed from $Cu_{2.5}SO_4(OH)_3{\cdot}2H_2O$ to $Cu_4SO_4(OH)_6$, and the morphology is transformed from yolk/shell microsphere to stacked microsheets (Supporting Information, Figure S11). As for the CHS@$Cu_3(BTC)_2$

DOI: 10.1021/am508079j
ACS Appl. Mater. Interfaces 2015, 7, 4667−4674

products, the phase and morphology can be retained even after three months, which is attributed to the stabilizing effect of $Cu_3(BTC)_2$ shell to the CHS core (Supporting Information, Figure S12).

Recently, heterogeneous catalysis in flow has attracted great attention due to its advantages for easy automation, saving energy, and environment protection.[46−49] However, one of the challenges in utilizing flow technology in heterogeneous catalysis is the preparation of solid-supported catalysts with good catalytic activity under flow conditions.[47] As for the CHS@$Cu_3(BTC)_2$ products, the CHS core serves as the active catalytic site, the $Cu_3(BTC)_2$ shell with a large surface area and high porosity enriches the reactants around the MPs as well as promoting the reaction, and the cavity between provides a microreaction environment for efficient catalysis. Further, the solid-core−porous-shell structure can avoid the accumulation of the active center and help the liquids to flow through, making CHS@$Cu_3(BTC)_2$ an ideal self-supported catalyst for heterogeneous catalysis in flow. A flow reactor for heterogeneous catalysis was designed and developed using CHS@$Cu_3(BTC)_2$ as immobilized stationary-phase catalyst. The organization of the principal design elements is illustrated in Figure 6. The reactant solution is injected into the column of the reactor packed with the CHS@$Cu_3(BTC)_2$, and the product solution is collected at the discharge port for GC analysis.

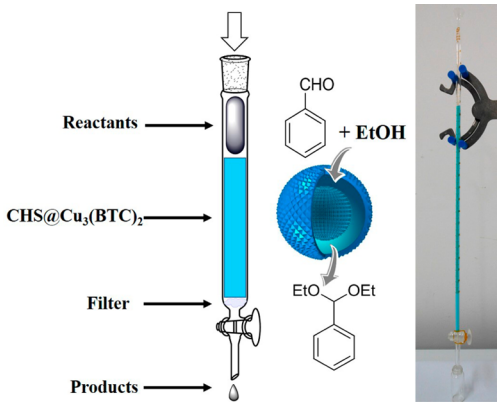

Figure 6. Schematic representation and photo image of the flow reactor using self-supported CHS@$Cu_3(BTC)_2$ catalyst.

Benzaldehyde was converted to benzaldehyde diethyl acetal with a good yield (up to 87%) and high selectivity (up to 99%) in a single pass of the packing catalysts (Table 2, entry 1), showing the excellent catalytic efficiency of CHS@$Cu_3(BTC)_2$ as self-supported catalyst. Furthermore, the acetalization of other aldehydes, such as 2-fluorobenzaldehyde, 4-fluorobenzaldehyde, *m*-tolualdehyde, *p*-tolualdehyde, *m*-anisaldehyde, *p*-anisaldehyde, and 2-furanaldehyde, also confirmed the general applicability of our self-supported CHS@$Cu_3(BTC)_2$ catalyst, and the results are summarized in Table 2. It can be observed that the aldehydes were converted to their corresponding diethyl acetals in high yield. Specifically, the conversion of *m*-substituted (Table 2, entry 2) and *o*-substituted benzaldehyde (Table 2, entries 4 and 6) is better than that of *p*-substituted benzaldehyde (Table 2, entries 3, 5, and 7) due to the steric hindrance, which made *p*-substituted substrate difficult to diffuse through the pore of the $Cu_3(BTC)_2$ shell.[50]

Table 2. Acetalization of Various Aldehydes Using the Flow Reactor with CHS@$Cu_3(BTC)_2$ as Immobilized Stationary-Phase Catalyst[a]

entry	substrate	product	conversion (%)	selectivity (%)
1		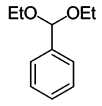	87	>99
2		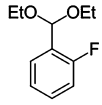	86	>99
3	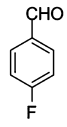	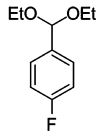	85	>99
4	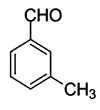	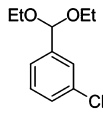	85	>99
5	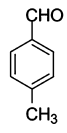	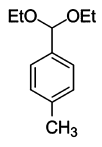	75	>99
6	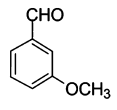	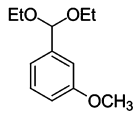	83	>99
7	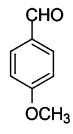	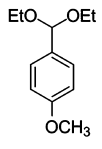	72	>99
8		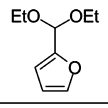	86	>99

[a]Reaction conditions: aldehydes and ethanol with a molar ratio of 1:80, at room temperature, a single pass.

Furanaldehyde is also well-acetalized to its corresponding diethyl acetals in good yields (ca. 86%) (Table 2, entry 8).

4. CONCLUSIONS

A novel self-template and in situ conversion approach for fabricating hierarchical yolk/shell CHS@MOF was developed. First a homogeneous CHS yolk/shell template composed of an active shell and a stabilized core was designed and fabricated. The active shell can provide metal ions and in situ transforms into MOF crystal shell, and the relatively stabilized core acts as the template, retaining its own nature during the conversion of the shell. Our in situ self-assembly strategy provided a general synthetic method for the preparation of multifunctional hybrid MP/NP@MOF with tailored structure, size, and properties by regulating the solvent composition and temperature. Finally, a flow reaction system using CHS@MOF self-supported catalyst was developed, which demonstrated excellent catalytic perform-

DOI: 10.1021/am508079j
ACS Appl. Mater. Interfaces 2015, 7, 4667−4674

ance for aldehyde acetalization due to the unique advantage in structure and function of the CHS@MOF.

■ ASSOCIATED CONTENT

Supporting Information

Additional characterization data, including SEM images, elemental mapping, FTIR patterns, TG curves, and XRD patterns. This material is available free of charge via the Internet at http://pubs.acs.org.

■ AUTHOR INFORMATION

Corresponding Authors

*E-mail: gewang@mater.ustb.edu.cn. (G.W.)
*E-mail: wdong@ustb.edu.cn. (W.D.)

Author Contributions

The manuscript was written through contributions of all authors. All authors have given approval to the final version of the manuscript.

Notes

The authors declare no competing financial interest.

■ ACKNOWLEDGMENTS

We thank the National Natural Science Foundation of China (Grant No. 51272028) and the National High Technology Research and Development program of China (No. 2013AA031702) for financial support.

■ ABBREVIATIONS

CHS, copper hydroxysulfates ($Cu_{2.5}SO_4(OH)_3{\cdot}2H_2O$)
BTC, 1,3,5-benzenetricarboxylate
MOF, metal−organic frameworks

■ REFERENCES

(1) Zhong, C. J.; Mathew, M. M. Core-Shell Assembled Nanoparticles as Catalysts. *Adv. Mater.* **2001**, *13*, 1507−1511.
(2) Salgueiriño-Maceira, V.; Correa-Duarte, M. A. Increasing the Complexity of Magnetic Core/Shell Structured Nanocomposites for Biological Applications. *Adv. Mater.* **2007**, *19*, 4131−4144.
(3) Wei, S.; Wang, Q.; Zhu, J.; Sun, L.; Lin, H.; Guo, Z. Multifunctional Composite Core-Shell Nanoparticles. *Nanoscale* **2011**, *3*, 4474−4502.
(4) Liu, J.; Qiao, S. Z.; Chen, J. S.; Lou, X. W.; Xing, X. R.; Lu, G. Q. Yolk/Shell Nanoparticles: New Platforms for Nanoreactors, Drug Delivery and Lithium-ion Batteries. *Chem. Commun.* **2011**, *47*, 12578−12591.
(5) Bétard, A.; Fischer, R. A. Metal-Organic Framework Thin Films: From Fundamentals to Applications. *Chem. Rev.* **2012**, *112*, 1055−1083.
(6) Kuppler, R. J.; Timmons, D. J.; Fang, Q. R.; Li, J. R.; Makal, T. A.; Young, M. D.; Yuan, D.; Zhao, D.; Zhuang, W.; Zhou, H. C. Potential Applications of Metal-Organic Frameworks. *Coord. Chem. Rev.* **2009**, *253*, 3042−3066.
(7) Li, J. R.; Sculley, J.; Zhou, H. C. Metal-Organic Frameworks for Separations. *Chem. Rev.* **2012**, *112*, 869−932.
(8) O'Keeffe, M.; Yaghi, O. M. Deconstructing the Crystal Structures of Metal-Organic Frameworks and Related Materials into Their Underlying Nets. *Chem. Rev.* **2012**, *112*, 675−702.
(9) Meilikhov, M.; Yusenko, K.; Esken, D.; Turner, S.; Tendeloo, G. V.; Fischer, R. A. Metals@MOFs-Loading MOFs with Metal Nanoparticles for Hybrid Functions. *Eur. J. Inorg. Chem.* **2010**, *2010*, 3701−3714.
(10) Ke, F.; Zhu, J. F.; Qiu, L. G.; Jiang, X. Controlled Synthesis of Novel Au@MIL-100(Fe) Core-Shell Nanoparticles with Enhanced Catalytic Performance. *Chem. Commun.* **2013**, *49*, 1267−1269.
(11) Ke, F.; Qiu, L. G.; Yuan, Y. P.; Jiang, X.; Zhu, J. F. Fe_3O_4@MOF Core-Shell Magnetic Microspheres With a Designable Metal-Organic Framework Shell. *J. Mater. Chem.* **2012**, *22*, 9497−9500.
(12) Lee, H. J.; Cho, W.; Oh, M. Advanced Fabrication of Metal-Organic Frameworks: Template-Directed Formation of Polystyrene@ZIF-8 Core-Shell and Hollow ZIF-8 Microspheres. *Chem. Commun.* **2012**, *48*, 221−223.
(13) Qin, F. X.; Jia, S. Y.; Wang, F. F.; Wu, S. H.; Song, J.; Liu, Y. Hemin@Metal-Organic Framework with Peroxidase-Like Activity and Its Application to Glucose Detection. *Catal. Sci. Technol.* **2013**, *3*, 2761−2768.
(14) Ahmed, A.; Forster, M.; Clowes, R.; Bradshaw, D.; Myers, P.; Zhang, H. Silica SOS@HKUST-1 Composite Microspheres as Easily Packed Stationary Phases for Fast Separation. *J. Mater. Chem. A* **2013**, *1*, 3276−3286.
(15) Sorribas, S.; Zornoza, B.; Téllez, C.; Coronas, J. Ordered Mesoporous Silica-(ZIF-8) Core-Shell Spheres. *Chem. Commun.* **2012**, *48*, 9388−9390.
(16) Koh, K.; Wong-Foy, A. G.; Matzger, A. J. MOF@MOF: Microporous Core-Shell Architectures. *Chem. Commun.* **2009**, *41*, 6162−6164.
(17) Kuo, C. H.; Tang, Y. L.; Chou, Y.; Sneed, B. T.; Brodsky, C. N.; Zhao, Z.; Tsung, C. K. Yolk-Shell Nanocrystal@ZIF-8 Nanostructures for Gas-Phase Heterogeneous Catalysis with Selectivity Control. *J. Am. Chem. Soc.* **2012**, *134*, 14345−14348.
(18) Liu, Y.; Tang, Z. Multifunctional Nanoparticle@MOF Core-Shell Nanostructures. *Adv. Mater.* **2013**, *25*, 5819−5825.
(19) Sabo, M.; Henschel, A.; Fröde, H.; Klemm, E.; Kaskel, S. Solution Infiltration of Palladium into MOF-5: Synthesis, Physisorption and Catalytic Properties. *J. Mater. Chem.* **2007**, *17*, 3827−3832.
(20) Aijaz, A.; Karkamkar, A.; Choi, Y. J.; Tsumori, N.; Ronnebro, E.; Autrey, T.; Shioyama, H.; Xu, Q. Immobilizing Highly Catalytically Active Pt Nanoparticles inside the Pores of Metal-Organic Framework: A Double Solvents Approach. *J. Am. Chem. Soc.* **2012**, *134*, 13926−13929.
(21) Dhakshinamoorthy, A.; Garcia, H. Catalysis by Metal Nanoparticles Embedded on Metal-Organic Frameworks. *Chem. Soc. Rev.* **2012**, *41*, 5262−5284.
(22) Li, P. Z.; Aranishi, K.; Xu, Q. ZIF-8 Immobilized Nickel Nanoparticles: Highly Effective Catalysts for Hydrogen Generation from Hydrolysis of Ammonia Borane. *Chem. Commun.* **2012**, *48*, 3173−3175.
(23) Lohe, M. R.; Gedrich, K.; Freudenberg, T.; Kockrick, E.; Dellmann, T.; Kaskel, S. Heating and Separation Using Nanomagnet-Functionalized Metal-Organic Frameworks. *Chem. Commun.* **2011**, *47*, 3075−3077.
(24) Park, T. H.; Hickman, A. J.; Koh, K.; Martin, S.; Wong-Foy, A. G.; Sanford, M. S.; Matzger, A. J. Highly Dispersed Palladium(II) in a Defective Metal-Organic Framework: Application to C-H Activation and Functionalization. *J. Am. Chem. Soc.* **2011**, *133*, 20138−20141.
(25) Houk, R. J. T.; Jacobs, B. W.; Gabaly, F. E.; Chang, N. N.; Talin, A. A.; Graham, D. D.; House, S. D.; Robertson, I. M.; Allendorf, M. D. Silver Cluster Formation, Dynamics, and Chemistry in Metal-Organic Frameworks. *Nano Lett.* **2009**, *9*, 3413−3418.
(26) Sugikawa, K.; Furukawa, Y.; Sada, K. SERS-Active Metal-Organic Frameworks Embedding Gold Nanorods. *Chem. Mater.* **2011**, *23*, 3132−3134.
(27) Wei, Y.; Han, S.; Walker, D. A.; Fuller, P. E.; Grzybowski, B. A. Nanoparticle Core/Shell Architectures within MOF Crystals Synthesized by Reaction Diffusion. *Angew. Chem., Int. Ed.* **2012**, *51*, 7435−7439.
(28) Falcaro, P. A.; Hill, J.; Nairn, K. M.; Jasieniak, J.; Mardel, J. I.; Bastow, T. J.; Mayo, S. C.; Gimona, M.; Gomez, D.; Whitfield, H. J.; Ricco, R.; Patelli, A.; Marmiroli, B.; Amenitsch, H.; Colson, T.; Villanova, L.; Buso, D. A New Method to Position and Functionalize Metal-Organic Framework Crystals. *Nat. Commun.* **2011**, *2*, 237.
(29) Lu, G.; Li, S. Z.; Guo, Z.; Farha, O. K.; Hauser, B. G.; Qi, X. Y.; Wang, Y.; Wang, X.; Han, S. Y.; Liu, X. G.; DuChene, J. S.; Zhang, H.; Zhang, Q. C.; Chen, X. D.; Ma, J.; Loo, S. C. J.; Wei, W. D.; Yang, Y.

DOI: 10.1021/am508079j
ACS Appl. Mater. Interfaces 2015, 7, 4667−4674

H.; Hupp, J. T.; Huo, F. W. Imparting Functionality to a Metal-Organic Framework Material by Controlled Nanoparticle Encapsulation. *Nat. Chem.* **2012**, *4*, 310−316.
(30) He, L.; Liu, Y.; Liu, J.; Xiong, Y.; Zheng, J.; Liu, Y.; Tang, Z. Core-Shell Noble-Metal@Metal-Organic-Framework Nanoparticles with Highly Selective Sensing Property. *Angew. Chem., Int. Ed.* **2013**, *52*, 3741−3745.
(31) Khaletskaya, K.; Reboul, J.; Meilikhov, M.; Nakahama, M.; Diring, S.; Tsujimoto, M.; Isoda, S.; Kim, F.; Kamei, K.; Fischer, R. A.; Kitagawa, S.; Furukawa, S. Integration of Porous Coordination Polymers and Gold Nanorods into Core-Shell Mesoscopic Composites toward Light-Induced Molecular Release. *J. Am. Chem. Soc.* **2013**, *135*, 10998−11005.
(32) Moon, H. R.; Lim, D. W.; Suh, M. P. Fabrication of Metal Nanoparticles in Metal-Organic Frameworks. *Chem. Soc. Rev.* **2013**, *42*, 1807−1824.
(33) Tsuruoka, T.; Kawasaki, H.; Nawafune, H.; Akamatsu, K. Controlled Self-Assembly of Metal-Organic Frameworks on Metal Nanoparticles for Efficient Synthesis of Hybrid Nanostructures. *ACS Appl. Mater. Interfaces* **2011**, *3*, 3788−3791.
(34) Zhan, W. W.; Kuang, Q.; Zhou, J. Z.; Kong, X. J.; Xie, Z. X.; Zheng, L. S. Semiconductor@Metal-Organic Framework Core-Shell Heterostructures: A Case of ZnO@ZIF-8 Nanorods with Selective Photoelectrochemical Response. *J. Am. Chem. Soc.* **2013**, *135*, 1926−1933.
(35) Liu, Y. Y.; Zhang, W. N.; Li, S. Z.; Cui, C. L.; Wu, J.; Chen, H. Y.; Huo, F. W. Designable Yolk-Shell Nanoparticle@MOF Petalous Heterostructures. *Chem. Mater.* **2014**, *26*, 1119−1125.
(36) Gao, H. Y.; Wang, G.; Luan, Y.; Chaikittikul, K.; Zhang, X. W.; Yang, M.; Dong, W. J.; Shi, Z. A Fast Synthesis of Hierarchical Yolk-Shell Copper Hydroxysulfates at Room Temperature with Adjustable Sizes. *CrystEngComm* **2014**, *16*, 2520−2526.
(37) Huang, K.; Wang, J. J.; Wu, D. F.; Lin, S. Copper Hydroxyl Sulfate as Heterogeneous Catalyst for the Catalytic Wet Peroxide Oxidation of Phenol. *RSC Adv.* **2015**, *5*, 8455−8462.
(38) Majano, G.; Pérez-Ramírez, J. Scalable Room-Temperature Conversion of Copper (II) Hydroxide into HKUST-1 ($Cu_3(btc)_2$. *Adv. Mater.* **2013**, *25*, 1052−1057.
(39) Wee, L. H.; Lohe, M. R.; Janssens, N.; Kaskel, S.; Martens, J. A. Fine Tuning of the Metal-Organic Framework $Cu_3(BTC)_2$ HKUST-1 Crystal Size in the 100 nm to 5 Micron Range. *J. Mater. Chem.* **2012**, *22*, 13742−13746.
(40) Decoste, J. B.; Peterson, G. W.; Smith, M. W.; Stone, C. A.; Willis, C. R. Enhanced Stability of Cu-BTC MOF via Perfluorohexane Plasma-Enhanced Chemical Vapor Deposition. *J. Am. Chem. Soc.* **2012**, *134*, 1486−1489.
(41) Zhu, Q.; Zhang, M.; Ma, Q. Copper-Based Foliar Fertilizer and Controlled Release Urea Improved Soil Chemical Properties, Plant Growth and Yield of Tomato. *Sci. Hortic.* **2012**, *143*, 109−114.
(42) Wu, Y.; Zhou, N. L.; Li, W. H.; Gu, H.; Fan, Y. T.; Yuan, J. Long-Term and Controlled Release of Chlorhexidine-Copper(II) from Organically Modified Montmorillonite (OMMT) Nanocomposites. *Mater. Sci. Eng., C* **2013**, *33*, 752−757.
(43) Dhakshinamoorthy, A.; Alvaro, M.; Garcia, H. Metal Organic Frameworks as Solid Acid Catalysts for Acetalization of Aldehydes with Methanol. *Adv. Synth. Catal.* **2010**, *352*, 3022−3030.
(44) De, S. K.; Gibbs, R. A. Ruthenium (III) chloride-catalyzed chemoselective synthesis of acetals from aldehydes. *Tetrahedron Lett.* **2004**, *45*, 8141−8144.
(45) Velusamy, S.; Punniyamurthy, T. Cobalt (II)-catalyzed chemoselective synthesis of acetals from Aldehydes. *Tetrahedron Lett.* **2004**, *45*, 4917−4920.
(46) Liu, X. Y.; Unal, B.; Jensen, K. F. Heterogeneous Catalysis with Continuous Flow Microreactors. *Catal. Sci. Technol.* **2012**, *2*, 2134−2138.
(47) Zhao, D. B.; Ding, K. L. Recent Advances in Asymmetric Catalysis in Flow. *ACS Catal.* **2013**, *3*, 928−944.
(48) Obermayer, D.; Balu, A. M.; Romero, A. A.; Goessler, W.; Luque, R.; Kappe, C. O. Nanocatalysis in Continuous Flow: Supported Iron Oxide Nanoparticles for the Heterogeneous Aerobic Oxidation of Benzyl Alcohol. *Green Chem.* **2013**, *15*, 1530−1537.
(49) Shi, L.; Wang, X. W.; Sandoval, C. A.; Wang, Z. H.; Li, J.; Wu, J.; Yu, L. T.; Ding, K. L. Development of a Continuous-Flow System for Asymmetric Hydrogenation Using Self-Supported Chiral Catalysts. *Chem.—Eur. J.* **2009**, *15*, 9855−9867.
(50) Chmelik, C.; Karger, J.; Wiebcke, M.; Caro, J.; Van Baten, J. M.; Krishna, R. Adsorption and Diffusion of Alkanes in CuBTC Crystals Investigated Using Infra-Red Microscopy and Molecular Simulations. *Microporous Mesoporous Mater.* **2009**, *117*, 22−32.

DOI: 10.1021/am508079j
ACS Appl. Mater. Interfaces 2015, 7, 4667−4674